# Computing geometric feature sizes for algebraic manifolds

Sandra Di Rocco[1], Parker B. Edwards[2], David Eklund[3], Oliver Gäfvert[4], and Jonathan D. Hauenstein[2]

[1]*Department of Mathematics, KTH, 10044, Stockholm, Sweden*
[2]*Department of Applied and Computational Mathematics and Statistics, University of Notre Dame, Notre Dame, IN, USA*
[3]*RISE, Research Institutes of Sweden, Isafjordsgatan 22, 16440, Kista, Sweden*
[4]*Mathematical Institute, University of Oxford, United Kingdom*

**Abstract**

We introduce numerical algebraic geometry methods for computing lower bounds on the reach, local feature size, and the weak feature size of the real part of an equidimensional and smooth algebraic variety using the variety's defining polynomials as input. For the weak feature size, we also show that non-quadratic complete intersections generically have finitely many geometric bottlenecks, and describe how to compute the weak feature size directly rather than a lower bound in this case. In all other cases, we describe additional computations that can be used to determine feature size values rather than lower bounds.

**MSC2020:** 14Q20,14Q65, 55N31
**Keywords:** bottlenecks, reach, numerical algebraic geometry, topological data analysis, weak feature size

## 1 Introduction

Exploring the geometry of a given data set has proven to be a powerful tool in data analysis. For example, topological data analysis (TDA) aims to recover topological information of a data set such as connectedness or holes in its shape [18, 23, 35] and has been successfully applied to problems in a wide range of fields [36, 44, 60]. If the data set lies on a manifold that is algebraic, namely it lies on a geometric shape defined by algebraic equations, a more direct approach using computational algebraic geometry can be applied. In this case, the data set can be viewed as a sampling of the algebraic manifold, as shown in Figure 1, where it is important to find guarantees that the topology of the sample, i.e., the topology of the Vietoris-Rips complex defined by the data set correctly estimates the topology of the underlying algebraic manifold.

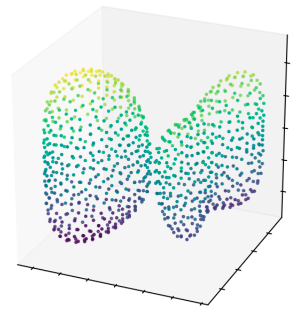

Figure 1: Dense sample from a quartic surface.

Topological and geometric data analysis algorithms frequently supply some form of the following guarantee: given a "dense enough" point sample from a space $X \subseteq \mathbb{R}^n$ as input, the algorithm correctly computes some geometric or topological property of $X$. The required density can be expressed in terms of certain invariants of the space $X$. The two most studied invariants are the *reach*, introduced by Federer [31], and the *weak feature size*, introduced by Grove and Shiohama in the context of Riemannian geometry [37, 38] and significantly expanded upon by Chazal and Lieutier for use in sampling and other computational geometry applications [20, 21]. These invariants are of considerable importance for persistent homology and reconstruction methods [4, 16, 21, 22, 25, 26, 47, 53].

In most settings, geometric feature sizes can only be estimated since a full specification of the space $X$ is not available. As a result, few examples of fully specified spaces with explicitly computed weak feature size have previously appeared. Algorithms computing these invariants and thus geometrical theories for efficient computations are an important area of study in applied geometry. This paper aims at providing some answers in this direction using numerical algebraic geometric methods, e.g. see [10, 56].

Throughout this paper, nonempty and compact algebraic manifolds $X = V(F) \cap \mathbb{R}^n$ are considered, where $F = \{f_1, f_2, \ldots, f_m\}$ is a system consisting of polynomials in $\mathbb{R}[x_1, \ldots, x_n]$ and $V(F) = \{x \in \mathbb{C}^n \mid F(x) = 0\}$. Section 2 presents necessary background on feature sizes. The distance-to-X function $d_X : \mathbb{R}^n \to \mathbb{R}$, defined as $d_X(z) = \inf_{x \in X} \|x - z\|$, is not differentiable everywhere in $\mathbb{R}^n$ for most spaces $X$. Grove [37] constructed an analog of Morse theory defining *critical points of* $d_X$ or *geometric bottlenecks* of $X$ as those points $z \in \mathbb{R}^n \setminus X$ which are in the convex hull of their closest points on $X$. The *weak feature size* is the infimum of all the *critical values* of $d_X$. The critical values of $d_X$ are those values $d_X(z)$ where $z$ is a geometric bottleneck (see Definition 2.3).

**Example.** Consider the ellipsoid $X \subseteq \mathbb{R}^3$ defined by $x_1^2 + x_2^2 + x_3^2/2 = 1$ as depicted in Figure 2. It has a single geometric bottleneck at the origin (red point).

We will see in Section 4 that the number of convex hulls of closest points which contain a geometric bottleneck crucially impacts computations. The ellipsoid in Figure 2 is an example that poses difficulties, as it has a one-dimensional locus of convex hulls along the $(x_1, x_2)$-plane which contain the origin. They are depicted with black segments connecting green antipodal points on the unit circle in the $(x_1, x_2)$-plane.

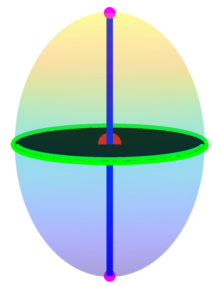

Figure 2: Ellipsoid

Algebraic conditions also detect that the origin is contained in the convex hull of its furthest points on $X$, which lies along the $x_3$-axis with blue segments connecting the magenta points at $(0, 0, \pm\sqrt{2})$ in Figure 2.

Using a combination of geometric arguments, the Tarski-Seidenberg Theorem, and Sard's Theorem, Fu proved that the set of critical values of $d_X$ is finite when $X$ is semi-algebraic [33]. This implies that the weak feature size is always positive. In the ellipsoid example, the weak feature size is 1. This theorem strongly motivates studying the weak feature size as it applies even when $X$ is not smooth nor equidimensional. The proof, however, does not suggest a feasible algorithm for computing the critical values of $d_X$.

In Section 3, we describe a method to compute the reach of $X$ as well as the *local feature size* [3] of $X$ at a point $w \in \mathbb{R}^n$ given the defining polynomials $F$ as input. Numerical computations can compute these quantities to arbitrary precision via our approach. Moreover, if the input depends on rational numbers, exactness recovery methods such as [8] can refine the numerical results to extract exact information. For example, we use exactness recovery methods in Example 2.4 to determine exact expressions for the reach of a particular space.

**Theorem** (3.10, 3.11)**.** *For both the reach and the local feature size, one can utilize the finite set of points computed via a single parameter homotopy [50] on a polynomial system constructed using first-order critical conditions to obtain a nontrivial lower bound. Using additional reality testing, one can determine the value of the reach and the local feature size.*

To the best of our knowledge, these provide the first algorithms that can compute these quantities for algebraic manifolds of arbitrary codimension.

Section 4 is dedicated to constructing a theory and algorithms for computing the weak feature size. We apply a wholly algebraic framework to this problem when $X$ is the real part of a smooth and equidimensional algebraic variety. The resulting theory yields an alternative proof of Fu's Theorem in this setting as well as a method for computing bounds on the weak feature size.

**Theorem** (4.8, 4.10)**.** *A lower bound on the weak feature size can be obtained using the union of the finite set of points computed via $n$ parameter homotopies [50]. Using additional reality testing, one can determine the value of the weak feature size.*

**Example.** The ellipsoid example above has a geometric bottleneck with infinitely many closest points. Although the previous theorem applies to that case, it is often more desirable from a numerical conditioning standpoint to consider nonsingular isolated solutions to well-constrained systems. Consider the perturbation defined by $x^2 + y^2 + z^2/2 + xz/7 = 1$, illustrated in Figure 3. In this case, only three convex hulls containing the geometric bottleneck at the origin contribute to algebraic computations. Black segments connect the origin to green points, which are distance minimizers.

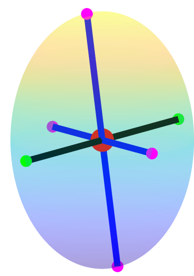

Figure 3: Perturbation of ellipsoid

This example's behavior is the typical result of a perturbation in a rigorous sense. By applying the celebrated Alexander-Hirschowitz Theorem [2] on the expected dimension of the secant variety of the Veronese embedding, one obtains a description of the generic behavior of geometric bottlenecks as summarized in the following.

**Theorem** (4.14). *Non-quadratic generic complete intersections have finitely many critical points, i.e., finitely many geometric bottlenecks.*

As a consequence, we construct algorithms using homotopy continuation to compute the weak feature size with arbitrary precision. Examples are presented in Section 5. A Julia package which implements these algorithms for general use via `HomotopyContinuation.jl` [15] is available at https://github.com/P-Edwards/HomologyInferenceWithWeakFeatureSize.jl. We also use `Bertini` [11] implementations. Data, scripts, and input files for all examples are available at https://github.com/P-Edwards/wfs-and-reach-examples.

## 1.1 Related work

Recent work on computing feature sizes in the algebraic setting mostly focused on computing lower bounds for the reach, motivated by a result of Amari et al. [1, Thm. 3.4] which shows the reach of a compact manifold is determined by two distinct types of geometric behavior: regions of high curvature and "bottleneck structures," which we call "geometric 2-bottlenecks" (Definition 4.1). Breiding and Timme [14] observed that a straightforward computation can find the maximal curvature of an implicitly defined plane curve and Horobeţ [45] studied the problem in greater generality by investigating an algebraic variety's critical curvature degree. Horobeţ and Weinstein [46] studied related theoretical problems in the context of "offset filtrations" and, in particular, showed that the reach is algebraic over $\mathbb{Q}$ for real algebraic manifolds defined by polynomials with rational coefficients. The third author [30] studied computing 2-bottlenecks with numerical algebraic geometry while Weinstein together with the first and third authors [28] developed formulas for the number of algebraic 2-bottlenecks of a smooth algebraic variety in terms of polar and Chern classes. Moreover, in [27] a special case of Theorem 4.14 for 2-bottlenecks is shown using a different approach.

Lowering the theoretical complexity of computing the Betti numbers and related invariants of semi-algebraic sets from a list of defining polynomials comprises a rich and ongoing topic of study in real algebraic geometry, e.g., the references [5, 6, 16] more extensively characterize recent progress in this area. The resulting algorithms are challenging to implement efficiently and, to the best of our knowledge, no general implementations are available. We take a distinct approach to homology inference that is complementary by focusing on producing efficient implementations rather than lowering complexity bounds.

# 2 Background and Preliminaries

The following summarizes the elements from the theory of distance functions and geometric feature sizes, particularly for semi-algebraic sets, necessary to state our results. In this paper, the distance between two points $x, z \in \mathbb{R}^n$ is the Euclidean distance:

$$d(x,z) = \|x - z\| = \sqrt{\sum_{i=1}^{n} (x_i - z_i)^2}.$$

For any nonempty subset $S \subseteq \mathbb{R}^n$, let $d_S : \mathbb{R}^n \to \mathbb{R}$ denote the distance-to-$S$ function, namely $d_S(z) = \inf_{s\in S} \|s - z\|$. For any non-negative $\varepsilon$, let $S^\epsilon = d_S^{-1}[0, \epsilon]$. For a nonempty and compact subset $X \subseteq \mathbb{R}^n$ and for any $z \in \mathbb{R}^n$, let $\pi_X(z) = \{x \in X \mid d_X(z) = d(x,z)\}$ be the set of points in $X$ with minimal distance to $z$.

**Definition 2.1.** The *medial axis* of $X$ is

$$\mathcal{M}_X = \overline{\{z \in \mathbb{R}^n \mid \#\pi_X(z) > 1\}}.$$

Equivalently, $\mathcal{M}_X$ is the (Euclidean) closure of the set of points in $\mathbb{R}^n$ that have at least 2 closest points in $X$.

Naturally, one can consider subsets of the medial axis based on the number of closest points. That is, for $k \geq 2$, $\mathcal{M}_{X,k} = \overline{\{z \in \mathbb{R}^n \mid \#\pi_X(z) \geq k\}}$ is the *$k$-medial axis* where $\mathcal{M}_X = \mathcal{M}_{X,2}$.

**Definition 2.2.** The function $d_{\mathcal{M}_X} : \mathbb{R}^n \to \mathbb{R} \cup \{\infty\}$ is also called the *local feature size* function of $X$ [3], denoted lfs. For $w \in \mathbb{R}^n$, $\mathrm{lfs}(w)$ is the *local feature size at $w$*. The function lfs takes value $\infty$ if $\mathcal{M}_X = \emptyset$, e.g., if $X$ is convex. The *reach* of $X$ [31] is defined as

$$\tau_X = \min_{x\in X} \mathrm{lfs}(x).$$

**Definition 2.3.** A point $z \in \mathbb{R}^n \setminus X$ is a *critical point of $d_X$* [37, 38] or a *geometric bottleneck*[1] of $X$ if $z$ is in the convex hull of $\pi_X(z)$. The *weak feature size* [21] of $X$ is defined as:

$$\mathrm{wfs}(X) = \inf_{z\in \mathrm{crit}(d_X)} d_X(z)$$

[1]This term is new and agrees with that used in recent work on this subject in the algebraic context [1, 14, 27, 28, 30]. It additionally distinguishes these points from other types of critical points which arise in this setting.

where $\mathrm{crit}(d_X)$ denotes the set of critical points of $d_X$.

Notice that $\mathrm{crit}(d_X)$ is a subset of $\mathcal{M}_X$, so that $\tau_X \leq \mathrm{wfs}(X)$. Also notice that the above condition can be phrased in terms of well-centered simplices. The convex hull of a set of at most $n+1$ affinely independent points in $\mathbb{R}^n$ is a *well-centered simplex* if its circumcenter lies in its interior [57]. A point $z \in \mathbb{R}^n \setminus X$ is a geometric bottleneck of $X$ if it is the circumcenter of a well-centered simplex with vertices in $\pi_X(z)$.

**Example 2.4.** To illustrate the previous definitions, consider the plane curve $C \subseteq \mathbb{R}^2$ defined by $d(x,p_1)^2 \cdot d(x,p_2)^2 = 2$ where $p_1 = (1,0)$ and $p_2 = (-1,0)$. The curve $C$ is called a *Cassini oval* with 2 foci and shown in Figure 4(a) along with its medial axis (cyan curve) and bottlenecks (red points). These types of curves, with a concentration on examples bearing more resemblance to an ellipse than the one we consider, were proposed by Cassini in the late 17$^{\text{th}}$ century as candidates for planetary orbits [19, p. 36].[2] The medial axis $\mathcal{M}_C$ consists of three segments along the coordinate axes, namely

$$\begin{aligned} &(a,0) \quad \text{for} \quad a \in \left[-\sqrt{2\sqrt{2}-2}, \sqrt{2\sqrt{2}-2}\right] \quad \text{and} \\ &(0,b) \quad \text{for} \quad b \in \left(-\infty, -\sqrt{2\sqrt{2}+2}\right] \cup \left[\sqrt{2\sqrt{2}+2}, \infty\right). \end{aligned}$$

The reach is $\tau_C = \sqrt{\sqrt{2}-1} \approx 0.6436$ attained at the origin and $\left(\pm\sqrt{2\sqrt{2}-2}, 0\right)$. There are three bottlenecks, namely the origin and $(\pm\sqrt{1/2}, 0)$ each with two closest points in $C$, with the weak feature size being $\mathrm{wfs}(C) = \sqrt{\sqrt{2}-1}$ attained at the origin. Hence, $\tau_C = \mathrm{wfs}(C)$.

Similarly, consider the plane curve $C' \subseteq \mathbb{R}^2$ defined by $d(x,r_1)^2 \cdot d(x,r_2)^2 \cdot d(x,r_3)^2 = 2$ where $r_1 = (1,0)$, $r_2 = (-1/2, \sqrt{3}/2)$, and $r_3 = (-1/2, -\sqrt{3}/2)$. The curve $C'$ is called a *Cassini oval* with 3 foci and is shown in Figure 4(b) along with its medial axis (cyan curve) and bottleneck (red point) at the origin which has three closest points in $C'$. The reach is

$$\tau_{C'} = \frac{\sqrt[3]{64 - 26\sqrt{2}}}{7} \approx 0.4298$$

attained at the three points on the end of the medial axis in the interior of $C'$. The weak feature size is $\mathrm{wfs}(C') = \sqrt[3]{\sqrt{2}-1} \approx 0.7454$ attained at the origin. Hence, $\tau_{C'} < \mathrm{wfs}(C')$.

We note that the exact values for the reach were computed by using the results of the numerical computation in Example 3.12 together with the exactness recovery method in [8] yielding minimal polynomials of $x^4+2x^2-1$ and $343x^6-128x^3+8$ for $\tau_C$ and $\tau_{C'}$, respectively. Hence, the algebraic degree of the reach is 4 and 6, respectively.

Distance functions $d_X : \mathbb{R}^n \to \mathbb{R}$ enjoy some properties similar to Morse functions in Morse theory [52] and justify studying the weak feature size in the algebraic setting. For the sake of analogy, recall that if $f : M \to \mathbb{R}$ is a Morse function on a compact manifold $M$ with critical points $C_f$ then, by a theorem of A. P. Morse [51] and Sard [54], $f(C_f)$ is finite. By a fundamental theorem of Morse theory (see, e.g., [49, Thm. 3.1]), if $f(C_f) \cap [r_1, r_2] = \emptyset$ then

[2] This 1693 publication of Cassini's is the earliest to which we could trace this example, but, e.g., Yates [61] dates Cassini's study of these ovals to the earlier date of 1680 without citation.

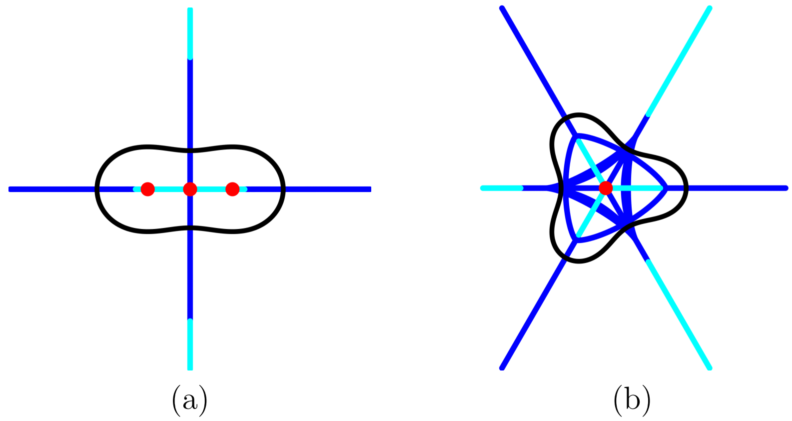

Figure 4: Black curve is the Cassini oval with (a) 2 foci and (b) 3 foci. The red points are geometric bottlenecks and the union of the cyan curves form the medial axis.

$f^{-1}(-\infty, r_1]$ is a deformation retract of $f^{-1}(-\infty, r_2]$. Analogously, if $X \subseteq \mathbb{R}^n$ is nonempty, semi-algebraic, and compact with set of geometric bottlenecks $B$, $d_X(B)$ is finite [33] and $\mathrm{wfs}(X) > 0$. If $d_X(B) \cap [r_1, r_2] = \emptyset$ with $r_1 \geq 0$ then $X^{r_1}$ is a deformation retract of $X^{r_2}$ [37].

The Morse Lemma implies that the set of critical points of a Morse function on a compact manifold is finite (see, e.g., [49, Cor. 2.3]). Nonetheless, the distance-to-$X$ function $d_X$ need not always have finitely many geometric bottlenecks even if $X$ is smooth, compact, and an algebraic subset of $\mathbb{R}^n$ (see, e.g., Example 3.14). More details are given in Section 4.

# 3 Algebraic medial axis, reach, and local feature size

The geometric definition of the medial axis and hence the reach and local feature size in Section 2 utilize a semi-algebraic condition via closest points. By replacing closest points with a criticality condition, the following provides an algebraic relaxation that is amenable to computational algebraic geometry over $\mathbb{C}$. As before, we assume that $X = V(F) \cap \mathbb{R}^n$ is nonempty and compact where $F$ is a polynomial system with real coefficients.

**Definition 3.1.** Let $F = \{f_1, \ldots, f_m\}$ be a system of polynomials in $n$ variables with real coefficients such that $V(F)$ is equidimensional and smooth of codimension $c$. The *medial axis correspondence* of $F$, denoted $M(F)$, is the algebraic subset of $\mathbb{C}^n \times \mathbb{C}^n \times \mathbb{C}^n$ given by:

$$\left\{ (x_1, x_2, z) \in \mathbb{C}^n \times \mathbb{C}^n \times \mathbb{C}^n \;\middle|\; \begin{array}{l} F(x_1) = F(x_2) = 0, \\ d(x_1, z)^2 = d(x_2, z)^2, \\ \mathrm{rank}[x_i - z \mid JF(x_i)^T] \leq c \quad \text{for } i = 1, 2 \end{array} \right\}$$

where $JF(p)$ is the Jacobian matrix of $F$ evaluated at $p$ and $[x_i - z \mid JF(x_i)^T]$ is the $n \times (m+1)$ matrix obtained by appending the indicated first column. If $\Delta$ is the algebraic set of points $(x_1, x_2, z) \in \mathbb{C}^n \times \mathbb{C}^n \times \mathbb{C}^n$ where any two of the entries are equal and $\pi_3 : (\mathbb{C}^n)^3 \to \mathbb{C}^n$ is projection onto the third factor, the *algebraic medial axis of* $F$ is $\overline{\pi_3(M(F) \setminus \Delta)}$, the Zariski closure of the image of the projection.

*Remark* 3.2. Let $z \in \mathcal{M}_X$, the medial axis of $X$. By definition, $\mathcal{M}_X = \{z \in \mathbb{R}^n \mid \exists (x_1, x_2 \in X)\; d(z, x_1) = d(z, x_2), x_1 \neq x_2 \neq z\}$. The conditions $\mathrm{rank}[x_i - z \mid JF(x_i)^T] \leq c$ defining

$M(F)$ enforce that for any $(x_1, x_2, z) \in M(F)$ the value $d(x_i, z)^2$ is a critical value of the function $d_X(\bullet, z) : \mathbb{R}^n \to \mathbb{R}$ and that $x_i \in V(F)$. Therefore, it is clear that $\mathcal{M}_X \subseteq \overline{\pi_3(M(F) \setminus \Delta)}$.

*Remark* 3.3. While the equations defining $M(F)$ in Definition 3.1 are sufficient for a general definition, the standard equations for the determinantal component $\operatorname{rank}[x_i - z | JF(x_i)^T] \leq c$ do not present $M(F)$ as a complete intersection and are correspondingly more challenging to work with computationally. In practice, we perform computations for the case $m = c$. In this case, we may consider an alternative algebraic correspondence $M'(F) \subseteq \mathbb{C}^n \times \mathbb{C}^n \times \mathbb{C}^n \times (\mathbb{C}^c)^2$ using a null space approach, e.g., see [9]. Let $(x_1, x_2, z) \in M(F)$. Since $V(F)$ is smooth of codimension $c$, for $i = 1, 2$, $\operatorname{rank}[x_i - z \mid JF(x_i)^T] \leq c$ is true if and only if

$$x_i - z + JF(x_i)^T \lambda_i = 0$$

for some $\lambda_i \in \mathbb{C}^c$. Define $M'(F)$ by

$$\left\{ (x_1, x_2, z, \lambda_1, \lambda_2) \in \mathbb{C}^n \times \mathbb{C}^n \times \mathbb{C}^n \times (\mathbb{C}^c)^2 \;\middle|\; \begin{array}{l} F(x_1) = F(x_2) = 0, \\ d(x_1, z)^2 = d(x_2, z)^2, \\ x_i - z + JF(x_i)^T \lambda_i \quad \text{for } i = 1, 2 \end{array} \right\}.$$

Denote by $\pi_3'$ the projection of $\mathbb{C}^n \times \mathbb{C}^n \times \mathbb{C}^n \times (\mathbb{C}^c)^2$ onto the third factor and set $\Delta' = \Delta \times (\mathbb{C}^c)^2$. Then it is direct that $\overline{\pi_3'(M'(F) \setminus \Delta')} = \overline{\pi_3(M(F) \setminus \Delta)}$. In following results where $M(F)$ appears, one can instead substitute $M'(F)$. There are $2c + 2n + 1$ equations in $3n + 2c$ variables which define $M'(F)$. One expects the algebraic medial axis $\overline{\pi_3'(M'(F) \setminus \Delta')}$ to be a hypersurface in $\mathbb{C}^n$.

*Remark* 3.4. As with the medial axis, one can consider subsets of the algebraic medial axis based on the number of equidistant critical points. That is, for $k \geq 2$, the *$k$-medial axis correspondence of $F$*, denoted $M_k(F)$, is the algebraic subset of $(\mathbb{C}^n)^k \times \mathbb{C}^n$ of points $(x_1, \ldots, x_k, z)$ which satisfy the equations:

$$\begin{array}{c} F(x_i) = 0 \\ \operatorname{rank}[x_i - z \mid JF(x_i)^T] \leq c \end{array} \quad \text{for } i = 1, \ldots, k \;\; \text{and } d(x_1, z)^2 = d(x_j, z)^2 \;\; \text{for } j = 2, \ldots, k.$$

If $\Delta_k$ is the subset of points $(x_1, \ldots, x_k, z) \in (\mathbb{C}^n)^k \times \mathbb{C}^n$ where any two of the entries are equal, the *algebraic $k$-medial axis of $F$* is the closure of the image of the projection of $M_k(F) \setminus \Delta$ onto its last factor. In particular, the algebraic medial axis is the algebraic 2-medial axis.

**Example 3.5.** For the Cassini oval with 2-foci in Example 2.4, the algebraic medial axis is the union of the coordinate axes. Moreover, for both the Cassini oval with 2- and 3-foci in Figure 4, the cyan curves form the medial axis and the union of the blue and cyan curves form the algebraic medial axis.

**Example 3.6.** The algebraic medial axis of a general plane curve of degree $d \geq 2$ is also a plane curve. After randomly selecting coefficients, we used `Bertini` [11] to compute the degree of the algebraic medial axis for $2 \leq d \leq 9$ as shown in the following table:

| $d$ | degree of algebraic medial axis |
|---|---|
| 2 | 2 |
| 3 | 30 |
| 4 | 120 |
| 5 | 320 |
| 6 | 690 |
| 7 | 1302 |
| 8 | 2240 |
| 9 | 3600 |

In particular, for $2 \leq d \leq 9$, the degree of the algebraic medial axis for a general plane curve of degree $d$ is

$$\binom{d}{2}(d^2 + 3d - 8) = \frac{d(d-1)(d^2 + 3d - 8)}{2}$$

and we conjecture that this formula holds for all $d \geq 2$.

We can investigate the reach and local feature size by considering optimization problems on $M(F)$. The solution to $\min\{d(x_1, z)^2 \mid (x_1, x_2, z) \in M(F) \setminus \Delta, d(x_1, z)^2 > 0\}$, for instance, is a lower bound on the reach. By using first-order critical conditions on $M(F)$, i.e. Lagrange multipliers, we can define critical conditions for the reach and and local feature size. Note that, for instance, the first-order critical conditions for optimizing the function $D_M : M(F) \to \mathbb{C}$ defined by $D_M(x_1, x_2, z) = d(x_1, z)^2$ are defined by equations in the variables $(x_1, x_2, z) \in (\mathbb{C}^n)^3$ derived from rank-vanishing conditions for matrices constructed from the Jacobians both of the equations defining M(F) and the function $D_M$.

**Definition 3.7.** Let $F = \{f_1, \ldots, f_m\}$ be a system of polynomials in $n$ variables with real coefficients such that $V(F)$ is equidimensional and smooth of codimension $c$. The *critical reach correspondence* of $F$, denoted $C(F)$, is the algebraic subset of $M(F)$ defined by first-order critical conditions of $D_M$.

Additionally, for $w \in \mathbb{C}^n$, the *critical local feature size correspondence* of $F$ with respect to $w$, denoted $L(F, w)$, is the algebraic subset of $M(F)$ defined by first-order critical conditions of the function $D_w : M(F) \to \mathbb{C}$ defined by $D_w(x_1, x_2, z) = d(w, z)^2$.

*Remark* 3.8. Note that $C(F), L(F, w) \subseteq M(F)$. Since the reach and local feature size are defined as solutions to optimization problems restricted to the medial axis, they are captured in the critical reach and critical local feature size correspondences, respectively. More precisely, $\tau_X \in D_M(C(F) \setminus \Delta)$ and $\mathrm{lfs}(w) \in D_w(L(F, w) \setminus \Delta)$.

*Remark* 3.9. As in Remark 3.3, it is more straightforward to specify and compute with equations for $C(F)$ and $L(F, w)$ in the case $m = c$. In that case we can define an alternative correspondence $C'(F) \subseteq M'(F) \times \mathbb{P}^{2n+2c+1}$ for $C(F)$ (a similar construction works for $L(F, w)$). Let $F_M : (\mathbb{C}^n)^3 \times (\mathbb{C}^c)^2 \to \mathbb{C}^{2n+2c+1}$ be the system of polynomial equations defining $M'(F)$. Then, denoting elements of $\mathbb{P}^{2n+2c+1}$ by $[\delta_0, \delta_1]$ with $\delta_0 \in \mathbb{C}$ and $\delta_1 \in \mathbb{C}^{2n+2c+1}$, $C'(F)$

is defined by

$$\left\{ (x_1, x_2, z, \lambda_1, \lambda_2, [\delta_0, \delta_1]) \;\middle|\; \begin{array}{l} F(x_1) = F(x_2) = 0, \\ d(x_1, z)^2 = d(x_2, z)^2, \\ x_i - z + JF(x_i)^T \lambda_i \quad \text{for } i = 1, 2 \\ \nabla \left(d(x_1, z)^2\right)^T \delta_0 + (J(F_M)(x_1, x_2, z, \lambda_1, \lambda_2))^T \delta_1 = 0 \end{array} \right\}.$$

This is a well-constrained system consisting of $4c+5n+1$ equations. Similarly, we can define $L'(F, w)$ with

$$\nabla \left(d(w, z)^2\right)^T \delta_0 + (J(F_M)(x_1, x_2, z, \lambda_1, \lambda_2))^T \delta_1 = 0, F_M(x_1, x_2, z, \lambda_1, \lambda_2) = 0.$$

The correspondences $C'(F)$ and $L'(F, w)$ may be substituted for $C(F)$ and $L(F, w)$ in the following results with minor modifications.

**Theorem 3.10.** Let $F$ be a polynomial system such that $V(F)$ is smooth and equidimensional of codimension $c$.

(a) Let $D_M : M(F) \to \mathbb{C}$ be defined by $(x_1, x_2, z) \mapsto d(x_1, z)^2$. Then, $D_M$ is constant on every connected component $C$ of $C(F)$ with $C \not\subseteq \Delta$.

(b) Fix $w \in \mathbb{C}^n$ and let $D_w : M(F) \to \mathbb{C}$ be defined by $(x_1, x_2, z) \mapsto d(w, z)^2$. Then, $D_w$ is constant on every connected component $C_w$ of $L(F, w)$ with $C_w \not\subseteq \Delta$.

*Proof.* We prove (a) and omit a similar proof of statement (b). Let $I$ be an irreducible component of $M(F)$ with $I \not\subseteq \Delta$. Then $D_M$ is constant when restricted to $I$, which follows directly from the construction and the algebraic version of Sard's Theorem, e.g., see [56, Thm A.4.10]. Since irreducible components are connected, each connected component $C$ of $M(F)$ with $C \not\subseteq \Delta$ must be the union of irreducible components not contained in $\Delta$. Furthermore, any irreducible component which is not a connected component must intersect at least one other distinct irreducible component. Thus, the constancy of $D$ can be extended to connected components yielding (a). □

Let $\mathcal{C}(F)$ denote the union of connected components of $C(F)$ not contained in $\Delta$ and similarly for $\mathcal{L}(F, w)$. By Remark 3.8 the reach is a value of $D_M$ on $\mathcal{C}(F)$. In fact, it is the minimum positive critical value of $d(x_1, z)^2$ on $\mathcal{C}(F)$ for which there is a real point that attains that critical value. Since there can only be finitely many critical values, this immediately provides an approach to compute the reach as follows. First, one computes a finite set of points that contains at least one point in each connected component of $\mathcal{C}$. Then, one evaluates $d(x_1, z)^2$ on the finite set of points to obtain the finite set of critical values. Immediately from this algebraic computation, one has that the minimum of the positive critical values is a lower bound on the reach. To obtain the actual value of the reach, one would need to employ an additional reality test, e.g., [40], to test for the existence of real points on the corresponding connected components. By searching in an increasing order starting with the minimum positive critical value, the reach is determined when a real point exists on the corresponding connected components.

Using numerical algebraic geometry, e.g., see [10, 56], there are several approaches using homotopy continuation that can be used to compute a finite set of points containing at least one on each connected component. For example, parameter homotopies [50] can be used to provide such a set. By looking at a finer decomposition based on irreducibility rather than connectedness, one can compute a finite set of points containing at least one on each irreducible component using a first-order general homotopy [7]. Another approach is to utilize a sequence of homotopies based on using linear slicing via a cascade [55] or regenerative cascade [43]. This last approach actually computes witness point sets (see [10, 56] for more details) which can then be used directly for reality testing via [40] when one expects positive-dimensional components. When the set of critical points is finite, all approaches yield the entire set of critical points and reality testing simply decides the reality of each critical point.

A similar argument follows for the local feature size as well. Moreover, one can treat $w$ as a parameter and utilize a parameter homotopy [50] to perform this computation efficiently at many different points. We summarize this in the following.

**Corollary 3.11.** Let $F$ be a polynomial system in $n$ variables with real coefficients such that $V(F)$ is smooth and equidimensional of codimension $c$ and $X = V(F) \cap \mathbb{R}^n$ is nonempty and compact. Fix $w \in \mathbb{R}^n$ and let $D_M$ and $D_w$ be as in Theorem 3.10.

(a) Using a parameter homotopy [50], one can compute a finite set of points $S$ which contains at least one point in each connected component of $\mathcal{C}(F)$. Then,

$$0 < \min_{s \in S \text{ with } D_M(s) > 0} \sqrt{D_M(s)} \leq \tau_X. \tag{1}$$

(b) Using a parameter homotopy [50], one can compute a finite set of points $S_w$ which contains at least one point in each connected component of $\mathcal{L}(F, w)$. Then,

$$0 < \min_{s \in S_w \text{ with } D_w(s) > 0} \sqrt{D_w(s)} \leq \mathrm{lfs}(w). \tag{2}$$

Since these inequalities can be strict when a corresponding connected component contains no real points, additional reality testing can be used to identify and ignore such components to yield $\tau_X$ and $\mathrm{lfs}(w)$.

This section concludes with some illustrative examples. In particular, the Cassini oval with 3 foci in the following shows a strict inequality in which additional reality testing yields the correct value.

**Example 3.12.** Consider computing the reach for the Cassini ovals with 2 and 3 foci from Example 2.4. We utilized a parameter homotopy in the corresponding space of multihomogeneous systems. For the Cassini oval with 2 foci, the lower bound in (1) is approximately 0.6436 which is attained at three different critical points computed by the homotopy. As shown in Figure 5(a), all three are real and thus the lower bound in (1) is equal to the reach.

For the Cassini oval with 3 foci, the lower bound in (1) is approximately 0.3611. Since this arises from nonreal isolated solutions to the critical point system, this can easily be discarded as not being equal to the reach. The next two smallest positive critical values are approximately 0.3674 and 0.3868 which also arise from nonreal isolated solutions to the critical point system and thus can be discarded as not being equal to the reach. Finally,

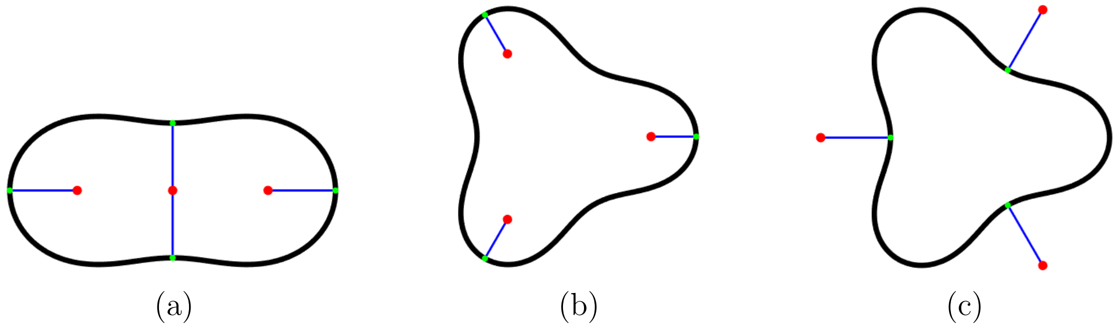


Figure 5: Reach attaining points for the Cassini oval with (a) 2 foci and (b) 3 foci. (c) Critical points arising from the algebraic closure of the reach for the Cassini oval with 3 foci.

the fourth smallest positive critical value is approximately 0.4298 which does arise from real solutions to the critical point system and is thus equal to the reach. The reach attaining points are shown in Figure 5(b).

As remarked in Example 2.4, the minimal polynomial for the reach of the Cassini oval with 3 foci is $343x^6 - 128x^3 + 8$. Since the critical reach correspondence is defined over the rational numbers, each root of this minimal polynomial is also a critical value. Figure 5(c) shows the critical points associated with the other real root which is approximately 0.6648.

**Example 3.13.** The medial axis of the unit circle defined by $x_1^2+x_2^2 = 1$ is the origin and thus the reach of 1 is attained at the origin. However, this reach attaining point is not isolated with respect to the critical reach correspondence since there are infinitely-many points on the unit circle where the reach is attained. Hence, the corresponding points computed via homotopy continuation need not be real. For example, using a multihomogeneous homotopy, 1 is the unique positive critical value arising from 78 distinct endpoints, none of which correspond with real points on the unit circle. Since 1 is the only positive critical value, it is the reach.

**Example 3.14.** The medial axis of the union of two concentric circles defined by

$$(x_1^2 + x_2^2 - 1)(x_1^2 + x_2^2 - 9) = 0$$

is the union of the origin and the circle centered at the origin of radius 2. Thus, the reach is 1 which is attained at every point on the medial axis as shown in Figure 6. For example, using a multihomogeneous homotopy, the minimum positive critical value is 1 which arises from 184 distinct endpoints. Of these, 168 correspond with the origin while the other 16 correspond with distinct points in $\mathbb{C}^2$ satisfying $x_1^2 + x_2^2 = 4$. From (1), this one homotopy shows that the reach is at least 1. For this example, it is easy to verify that there exist real critical points that yield a critical value of 1 which shows that the reach is indeed equal to 1.

# 4 Bottlenecks and weak feature size

The following expands upon the definition of geometric bottlenecks from Definition 2.3 and considers successive approximations of the weak feature size using *higher order bottlenecks*.

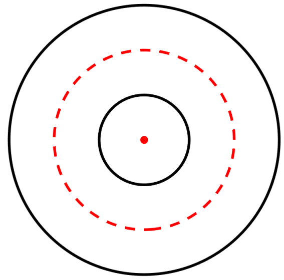

Figure 6: Reach obtained on a curve and a point for two concentric circles

**Definition 4.1.** Let $X$ be a compact subset of $\mathbb{R}^n$. A geometric bottleneck $z$ in $\mathrm{crit}(d_X)$ has *order* $k \geq 2$ if $z$ is a convex combination of $k$ affinely independent points in $\pi_X(z)$ and is not a convex combination of any fewer number of points in $\pi_X(z)$. We will often refer to such a point $z$ as a *geometric $k$-bottleneck* of $X$.

*Remark* 4.2. Definition 4.1 resembles a generalization of the index of critical points of a Morse function introduced by Gershokovich and Rubinstein [34]. The treatment by Bobrowski and Adler renders this connection clearer for distance functions [12, Def. 2.1], albeit for the case where $X$ is a finite point set. A geometric $k$-bottleneck of $X$ is a critical point of $d_X$ with index $k-1$ using that terminology. When $X$ is a finite set of points, this notion of index yields a decomposition similar to the classic cellular decomposition theorem of Morse theory (see, e.g., [49, Thm. 3.5] and [12, §4.2]). This does not extend to the case when $X$ is not finite. In particular, the Cassini oval with 2 foci in Example 2.4 and the unit circle in Example 3.13 are both counter examples. We use the term *order* rather than *index* to clarify that a Morse-type result does not apply in our setting.

Before considering the algebraic setting, the following highlights the relationship between geometric $k$-bottlenecks and weak feature size from Definition 2.3.

**Proposition 4.3.** If $X$ is a compact subset of $\mathbb{R}^n$, then every geometric bottleneck has order at most $n+1$ and

$$\mathrm{wfs}(X) = \inf_{z \text{ geom. } k\text{-bottleneck, } 2 \leq k \leq n+1} d_X(z).$$

*Proof.* Suppose that $z$ is a geometric bottleneck of $X$. Then, by definition, $z \in \mathrm{conv}(\pi_X(z))$. By Carathéodory's Theorem [17], $z$ is a convex combination of at most $n+1$ points in $\pi_X(z)$ which shows that the order of $z$ is at most $n+1$. □

*Remark* 4.4. From Proposition 4.3, it is natural to ask, for algebraic manifolds, if one must use all possible orders of geometric bottlenecks to determine the weak feature size or if one could use less, e.g., use only geometric 2-bottlenecks. The Cassini oval with 3 foci in Example 2.4 lies in $\mathbb{R}^2$ and has no geometric 2-bottlenecks. In particular, the weak feature size is attained at the origin, which is a geometric bottleneck of maximal order 3. Similar Cassini oval constructions generalize to higher dimensions and also generalize [27, Ex 3.4].

Following a similar approach as in Section 3, one can relax the conditions of a geometric $k$-bottleneck to obtain algebraic conditions amenable to computational algebraic geometry over $\mathbb{C}$. As before, we assume that $X = V(F) \cap \mathbb{R}^n$ is nonempty and compact where $F$ is a polynomial system with real coefficients.

**Definition 4.5.** Let $F = \{f_1, \ldots, f_m\}$ be a system of polynomials in $n$ variables with real coefficients such that $V(F)$ is equidimensional and smooth of codimension $c$ and $k \geq 2$. The $k^{\text{th}}$ *bottleneck correspondence* of $F$, denoted $B_k(F)$, is

$$\left\{ (x_1, \ldots, x_k, t_1, \ldots, t_k) \in (\mathbb{C}^n)^k \times \mathbb{C}^k \;\middle|\; \begin{array}{ll} \sum_{i=1}^k t_i = 1, & \\ z = \sum_{i=1}^k t_i x_i, & \\ d(x_1, z)^2 = d(x_j, z)^2 \quad \text{for } j = 2, \ldots, k & \\ F(x_i) = 0 & \text{for} \quad i = 1, \ldots, k. \\ \operatorname{rank}[x_i - z \mid JF(x_i)^T] \leq c & \end{array} \right\}.$$

Let $\Gamma_k \subset (\mathbb{C}^n)^k \times \mathbb{C}^k$ consist be the algebraic set defined by

$$\left\{ (x_1, \ldots, x_k, t_1, \ldots, t_k) \in (\mathbb{C}^n)^k \times \mathbb{C}^k \;\middle|\; \begin{array}{l} \text{Any } t_i = 0 \quad \text{for } i = 1, \ldots, k \\ \text{or} \\ \{x_1, \ldots, x_k\} \text{ is affinely dependent} \end{array} \right\}.$$

Consider the map $\rho_k : (\mathbb{C}^n)^k \times \mathbb{C}^k \to \mathbb{C}^n$ defined by $\rho_k(x_1, \ldots, x_k, t_1, \ldots, t_k) = \sum_{i=1}^k t_i x_i$. A point $z \in \mathbb{C}^n$ is an *algebraic $k$-bottleneck* of $V(F)$ if $z \in \rho_k(B_k(F) \setminus \Gamma_k)$. A *real algebraic $k$-bottleneck* of $V(F)$ is a point in $\mathbb{R}^n$ which is an algebraic $k$-bottleneck. Let $X = V(F) \cap \mathbb{R}^n$ and $R_{X,k} = X^k \times (0,1)^k \subset (\mathbb{R}^n)^k \times \mathbb{R}^k$. A *real algebraic $k$-bottleneck* of $X$ is a point in $\mathbb{R}^n$ in the image of $\rho_k((B_k(F) \cap R_{X,k}) \setminus \Gamma_k)$.

*Remark* 4.6. Following the notation of Definition 4.5, every geometric $k$-bottleneck of $X$ is a real algebraic $k$-bottleneck of $X$. In particular, one has the following relationship:

$$\{\text{geometric } k\text{-bottlenecks of } X\} \subseteq \{\text{real algebraic } k\text{-bottlenecks of } X\} \subseteq$$
$$\{\text{real algebraic } k\text{-bottlenecks of } V(F)\} \subseteq \{\text{algebraic } k\text{-bottlenecks of } V(F)\} = \rho(B_k(F) \setminus \Gamma_k).$$

Typically, these inclusions are strict as the examples in Section 5 exhibit. In particular, for the second inclusion, it is possible for the image of $\rho_k$ to be real for nonreal input.

**Example 4.7.** Consider computing the algebraic 2-bottlenecks for the perturbed ellipsoid $X \subseteq \mathbb{R}^3$ from the Introduction defined by $F = x_1^2 + x_2^2 + x_3^2/2 + x_1 x_3/7 - 1$. The set $B_2(F) \setminus \Gamma_2$ consists of three points up to symmetry, which are depicted in Figure 3 with the black segments corresponding to the geometric 2-bottleneck of $X$ while the blue segments correspond with real algebraic 2-bottlenecks of $X$ that are not geometric 2-bottlenecks of $X$.

## 4.1 Critical values

The following exhibits a result similar to Theorem 3.10.

**Theorem 4.8.** Let $F$ be a polynomial system such that $V(F)$ is smooth and equidimensional of codimension $c$. Let $k \geq 2$ and $D_k : B_k(F) \to \mathbb{C}$ be defined by

$$(x_1, \ldots, x_k, t_1, \ldots, t_k) \mapsto \frac{1}{k} \sum_{i=1}^k d\left(x_i, \rho_k(x_1, \ldots, x_k, t_1, \ldots, t_k)\right)^2.$$

Then, $D_k$ is constant on every connected component of $B_k(F) \setminus \Gamma_k$.

*Proof.* Similarly to Theorem 3.10, it suffices to show constancy for an irreducible component $C$ not contained in $\Gamma_k$.

The following shows that every point in $B_k(F) \setminus \Gamma_k$ is a critical point of $D_k$. Since $D_k|_C$ is an algebraic map of irreducible quasiprojective algebraic sets, it follows by the algebraic version of Sard's Theorem, e.g., [56, Thm A.4.10], that $D_k$ is not dominant, and therefore $D_k(C)$ is a single point because otherwise $C$ is not irreducible. Note that the critical points of $D_k$ are the same as those of $k \cdot D_k$ so we will consider $k \cdot D_k$ for simplicity.

Let $A_k(F) \subset (\mathbb{C}^n)^k \times \mathbb{C}^n$ be the set of $(x_1, \ldots, x_k, z)$ satisfying

$$\begin{array}{l} F(x_i) = 0 \;\text{ for } i = 1, \ldots, k, \\ d(x_1, z)^2 = d(x_j, z)^2 \;\text{ for } 2 \leq j \leq k. \end{array}$$

Clearly, there is an inclusion map $i : (B_k(F) \setminus \Gamma_k) \to A_k(F)$ given by

$$(x_1, \ldots, x_k, t_1, \ldots, t_k) \mapsto \left( x_1, \ldots, x_k, \sum_{i=1}^{k} t_i x_i \right).$$

By the chain rule, we need only prove that any point in the image of $i$ is a critical point of the map $D_k' : A_k(F) \to \mathbb{C}$ defined by $(x_1, x_2, \ldots, x_k, z) \mapsto \sum_{i=1}^{k} d(x_i, z)^2$. Since $V(F)$ is smooth and equidimensional, one may check directly that $A_k(F)$ has codimension $kc + k - 1$. By elementary row operations, one reduces the problem to showing that $(x_1, \ldots, x_k, z)$ is a critical point of $D_k'$ if the $(km + k) \times (kn + n)$ matrix

$$\begin{pmatrix}
JF(x_1) & 0 & 0 & 0 & 0 & \ldots & 0 \\
0 & JF(x_2) & 0 & 0 & 0 & \ldots & 0 \\
 & & & \vdots & & & \\
0 & 0 & 0 & \ldots & 0 & JF(x_k) & 0 \\
0 & -(x_2 - z)^T & 0 & \ldots & 0 & 0 & (x_2 - x_1)^T \\
0 & 0 & -(x_3 - z)^T & 0 & \ldots & 0 & (x_3 - x_1)^T \\
 & & & \vdots & & & \\
0 & 0 & 0 & \ldots & 0 & -(x_k - z)^T & (x_k - x_1)^T \\
(x_1 - z)^T & 0 & 0 & 0 & \ldots & 0 & (z - x_1)^T
\end{pmatrix}$$

has rank at most $kc + k - 1$ where $m$ is the number of polynomials in $F$. Suppose that $(x_1, \ldots, x_k, z) \in \operatorname{im}(i)$. Then the first $kn$ columns of this matrix contribute at most $kc$ to the dimension of the column space and the final $n$ columns contribute at most by $k - 1$ since $x_2 - x_1, \ldots, x_k - x_1$ span the affine hull of $x_1, \ldots, x_k$ and $z - x_1$ is in that affine hull. Altogether the rank of the matrix is at most $kc + k - 1$. □

*Remark* 4.9. For $k = 2$, this proof shows that the algebraic 2-bottlenecks of $V(F)$ correspond with a subset of the Zariski closure $C(F) \setminus \Delta$ where $C(F)$ is the critical reach correspondence. In contrast to $C(F)$, however, the correspondence $B_2(F)$ does not contain functions corresponding to the gradients of rank conditions. This is illustrated in Figure 5(a) for the Cassini oval with 2 foci.

As with Theorem 3.10 yielding Corollary 3.11, Theorem 4.8 provides the following.

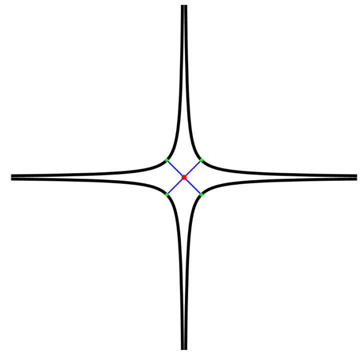

Figure 7: Real solutions of $x^2y^2 = 1$ with its geometric bottlenecks

**Corollary 4.10.** Let $F$ be a polynomial system in $n$ variables with real coefficients such that $V(F)$ is smooth and equidimensional of codimension $c$ and $X = V(F) \cap \mathbb{R}^n$ is nonempty and compact. For each $k = 2, \ldots, n+1$, one can use a parameter homotopy [50] to compute a finite set of points $E_k$ which contains at least one point in each connected component of $B_k(F) \setminus \Gamma_k$. Then,

$$0 < \min_{k=2,\ldots,n+1} \left( \min_{e \in E_k \text{ with } D_k(e) > 0} \sqrt{D_k(e)} \right) \leq \mathrm{wfs}(X). \tag{3}$$

Since this inequality can be strict when a corresponding connected component contains no real points, additional reality testing can be used to identify and ignore such components to yield $\mathrm{wfs}(X)$.

*Remark* 4.11. Compactness may be removed as a requirement in Theorem 4.8 and Corollary 4.10, but some care is necessary when $X = V(F) \cap \mathbb{R}^n$ is not compact. If $X$ is compact, then $X$ is a deformation retract of $X^\epsilon$ for some sufficiently small $\epsilon > 0$ since it is an absolute neighborhood retract [39, Cor 3.5], [48, Thm. 3]. As a non-compact example, consider $F = x^2y^2 - 1$ with $X$ shown in Figure 7. Theorem 4.8 shows that the weak feature size of $X = V(F) \cap \mathbb{R}^2$ inside any closed Euclidean ball of finite radius centered at the origin that intersects $X$ in $\mathbb{R}^2$ must be positive. By an explicit computation, one can see that the only contributors to the weak feature size in $B_2(F) \setminus \Gamma_2$ are isolated solutions as shown in Figure 7. The subtlety is that the manifold $V(F) \cap \mathbb{R}^2$ is not homotopy equivalent to any of its thickenings and thus it is not an absolute neighborhood retract.

**Example 4.12.** Consider the ellipsoid $X \subseteq \mathbb{R}^3$ defined by $F = x_1^2 + x_2^2 + x_3^2/2 - 1$ from the Introduction that is depicted in Figure 2. We consider computing the algebraic 2-bottlenecks using Corollary 4.10 in two different ways: using a parameter homotopy in the corresponding space of multihomogeneous systems and using a parameter homotopy from the perturbed ellipsoid computed in Example 4.7.

For the first approach, one obtains 6 points in $B_2(F) \setminus \Gamma_2$. Two of these points are real and equal up to symmetry. They correspond with the blue segments connecting the magenta points in Figure 2 at a distance of $\sqrt{2}$ from the origin, i.e., $D_2 = 2$. The other 4 points are nonreal and have $D_2 = 1$. These lie on a positive-dimensional component in $B_2(F) \setminus \Gamma_2$ containing the set $\{(x, -x, 1/2, 1/2)\}_{x \in V(x_1^2+x_2^2-1, x_3)}$ arising from antipodal points on the unit circle in the $(x_1, x_2)$-plane whose real points are shown in Figure 2. For this example, it is easy to verify that there exist real points on this component which are also geometric 2-bottlenecks.

For the second approach, we can consider the family of algebraic 2-bottlenecks for

$$F_t = x_1^2 + x_2^2 + x_3^2/2 + tx_1x_2 - 1.$$

Example 4.7 shows that, at the generic parameter value $t = 1/7$, $V(F_t)$ has three algebraic 2-bottlenecks. We then used a parameter homotopy to track these three solutions along the sufficiently general path defined by

$$t(s) = \frac{1}{7} \cdot \frac{\gamma s}{1 - s + \gamma s} \quad \text{where} \quad \gamma = 2 + 3\sqrt{-1}$$

as $s$ goes from 1 to 0. This yielded three real solutions which lie along the three coordinate axes. The two lying along the $x_1$ and $x_2$ coordinate axes have $D_2 = 1$ while the third that lies along the $x_3$ coordinate axis has $D_2 = 2$.

## 4.2 Critical points

The remainder of this section considers the finiteness of algebraic $k$-bottlenecks for general complete intersections of codimension $c$ in $\mathbb{C}^n$. Of course, we naturally assume that $n \geq 1$ and $1 \leq c \leq n$. Let $(d_1, \ldots, d_c) \in \mathbb{N}^c$ and consider $P_i = \mathbb{P}^{N_i}$ where $N_i = \binom{d_i+n}{d_i} - 1$ which is the parameter space of hypersurfaces in $\mathbb{C}^n$ of degree at most $d_i$. Furthermore, complete intersections in $\mathbb{C}^n$ of codimension $c$ and degree type $(d_1, \ldots, d_c)$ are parameterized by an open subset $U \subseteq \prod_{i=1}^{c} P_i$. Let $X_u$ denote the complete intersection in $\mathbb{C}^n$ corresponding to $u \in U$ and $F_u$ be the system of $c$ polynomials in $n$ variables that defines $X_u$.

**Definition 4.13.** For $k \geq 2$, the *$k$-bottleneck correspondence* for degree pattern $(d_1, \ldots, d_c)$, denoted $S_k$, is the set of points $(u, x_1, \ldots, x_k, t_1, \ldots, t_k) \in U \times (\mathbb{C}^n)^k \times \mathbb{C}^k$ such that

$$(x_1, \ldots, x_k, t_1, \ldots, t_k) \in B_k(F_u).$$

We will analyze $S_k$ via projections onto its factors. In particular, let $\pi : S_k \to (\mathbb{C}^n)^k \times \mathbb{C}^k$ and $\eta : S_k \to U$ be the projection maps. For any $u \in U$, the fiber $\eta^{-1}(u)$ is $\{u\} \times B_k(F_u)$.

The following provides a finiteness condition for algebraic $k$-bottlenecks. Since geometric $k$-bottlenecks are algebraic $k$-bottlenecks, this immediately implies a finiteness condition for geometric $k$-bottlenecks as well.

**Theorem 4.14.** Let $k \geq 2$ and $(d_1, \ldots, d_c) \in \mathbb{N}^c$ such that each $d_i \neq 2$. For general $u \in U$, the set of algebraic $k$-bottlenecks for $V(F_u)$ is finite. In particular, for general $u \in U$, $\eta^{-1}(u) \setminus \Gamma_k$ is finite.

The proof of this theorem is provided at the end of this section and follows from the Alexander-Hirschowitz Theorem [2], which is a result for homogeneous hypersurfaces. Thus, we need to move from affine space to projective space. In particular, $\mathbb{P}^N$ parameterizes homogeneous polynomials in $n + 1$ variables of degree $d$ where $N = \binom{d+n}{d} - 1$. For $a \in \mathbb{P}^N$, let $F_a(x_0, \ldots, x_n)$ denote the corresponding homogeneous polynomial of degree $d$.

Let $p_1, \ldots, p_k \in \mathbb{P}^n$ be general. The Alexander-Hirschowitz Theorem considers the dimension of the interpolation space of polynomials of degree $d$ having at least a double point at $p_i$, namely

$$I_{n,k} = \left\{ a \in \mathbb{P}^N \;\middle|\; F_a(p_i) = \frac{\partial F_a}{\partial x_j}(p_i) = 0 \text{ for } j = 1, \ldots, n \text{ and } i = 1, \ldots, k \right\}.$$

**Theorem 4.15** (Alexander-Hirschowitz [2])**.** The interpolation space $I_{n,k}$ has the *expected dimension*, i.e., $\dim(I_{n,k}) = \min\{(n+1)k - 1, N\}$, except for the following cases

- $d = 2, 2 \leq k \leq n$;
- $n = 2, d = 4, k = 5$;
- $n = 3, d = 4, k = 9$;
- $n = 4, d = 3, k = 7$;
- $n = 4, d = 4, k = 14$.

An equivalent statement of this theorem is that the $k$-secant variety of the $d^{\text{th}}$ Veronese embedding of $\mathbb{P}^n$, which we will call the $(n, d)$-Veronese variety $V_{n,d}$, has the expected dimension except for the listed exceptions.

*Remark* 4.16. Suppose that $p_1, \ldots, p_k, q_1, \ldots, q_k \in \mathbb{P}^n$ where $k \leq n+1$ are such that $p_1, \ldots, p_k$ and $q_1, \ldots, q_k$ each span a $(k-1)$-dimensional space. Let $I_p$ and $I_q$ denote the interpolation space $I_{n,k} \subseteq \mathbb{P}^N$ as defined above, respectively. Then, $I_p$ and $I_q$ have the same dimension. To see this, first note that there is a full rank linear map $L : \mathbb{P}^n \to \mathbb{P}^n$ such that $Lq_i = p_i$ for all $i$. More explicitly, complete $p_1, \ldots, p_k$ to a spanning set $p_1, \ldots, p_{n+1}$ of $\mathbb{P}^n$ and similarly for $q_1, \ldots, q_k$. Let $P = (p_1 \cdots p_{n+1})$ and $Q = (q_1 \cdots q_{n+1})$ be $(n+1) \times (n+1)$-matrices whose columns are the homogeneous coordinates of $p_1, \ldots, p_{n+1}$ and $q_1, \ldots, q_{n+1}$. Then $L$ is represented by $PQ^{-1}$.

The group $\mathrm{PGL}_n$ acts on the parameter space of hyper surfaces $\mathbb{P}^N$ as follows: for $T \in \mathrm{PGL}_n$, $Ta$ is given by the polynomial $F_a \circ T^{-1}$. Using this action and with $L$ as above, $LI_q = I_p$. In particular, by the chain rule $J(F_a \circ L)(q_i) = JF_a(p_i)L$ for all $i$ and $a \in \mathbb{P}^N$. This action and the Alexander-Hirschowitz Theorem yield a straightforward proof of the following.

**Lemma 4.17.** Let $p_1, \ldots, p_k \in \mathbb{P}^n$ with $k \leq n + 1$ and suppose that $p_1, \ldots, p_k$ span a $(k-1)$-dimensional subspace of $\mathbb{P}^n$. With notation as above, the interpolation space has the expected dimension except if $d = 2$ and $2 \leq k \leq n$.

**Proposition 4.18.** If the $k$-secant variety of the $(n, d)$-Veronese variety $V_{n,d}$ has the expected dimension for generic $p_1, \ldots, p_k \in \mathbb{P}^n$, then the $k(n+1)$ linear forms in $(a_0, \ldots, a_N)$ which comprise the entries of $JF_a(p_1), \ldots, JF_a(p_k)$ are independent.

*Proof.* Let $\nu(p) = \nu_{d,n}(p) = (p^j)_{\{j\}} \in V_{n,d}$. Then, the projective tangent space to $V_{n,d}$ at $\nu(p)$ is spanned by $\nu_{x_0}(p), \ldots, \nu_{x_n}(p)$ where $\nu_{x_i} = \frac{\partial \nu}{\partial x_i}$. The coefficients of the linear form $\frac{\partial F_a}{\partial x_i}(p)$ are the elements of the $(N+1)$-vector $\nu_{x_i}(p)$. $\square$

In order to show that a general complete intersection has a finite number of algebraic $k$-bottlenecks, we need to show that the generic fiber of the projection $\eta : S_k \to U$ is finite. We do this by first studying the dimension of the fibers of the projection $\pi : S_k \to (\prod_{i=1}^k \mathbb{C}^n) \times \mathbb{C}^k$.

**Lemma 4.19.** Let $k \geq 2$ and $(d_1, \ldots, d_c) \in \mathbb{N}^c$ such that each $d_i > 2$. If $(x_1, \ldots, x_k, t_1, \ldots, t_k) \in \pi(S_k) \setminus \Gamma_k$ then $\operatorname{codim}_U(\pi^{-1}(x_1, \ldots, x_k, t_1, \ldots, t_k)) = kn$.

*Proof.* By assumption, the equations

$$\sum_{i=1}^k t_i = 1, \quad z = \sum_{i=1}^k t_i x_i, \quad d(x_1, z)^2 = d(x_j, z)^2, \quad 2 \leq j \leq k$$

are satisfied. The fiber $\pi^{-1}(x_1, \ldots, x_k, t_1, \ldots, t_k)$ is the algebraic subset of $U$ defined by the conditions

$$x_i \in X_u \quad \text{and} \quad \operatorname{rank}[x_i - z \mid JF_u(x_i)^T] \leq c \quad \text{for } 1 \leq i \leq k.$$

First note that $x_i - z = \sum_{j=1, j \neq i}^k t_j(x_i - x_j)$ for all $i$. In particular, $x_i - z \neq 0$ because $\{x_i - x_j\}_{j=1, j\neq i}^k$ is linearly independent by assumption and none of $t_1, \ldots, t_k$ is 0. For all $i$, there subsequently exists a full rank $n \times n$ matrix $M_i$ such that $M_i(x_i - z) = e_1$, with $e_1$ the standard basis vector for $\mathbb{C}^n$. The fiber $\pi^{-1}(x_1, \ldots, x_k, t_1, \ldots, t_k)$ is equivalently defined by the conditions

$$F_u(x_i) = 0 \quad \text{and} \quad \operatorname{rank} \begin{bmatrix} 1 & 0 & \cdots & 0 \\ 0 & & & \\ \vdots & & (M_i(JF_u(x_i)^T))' & \\ 0 & & & \end{bmatrix} \leq c \quad \text{for } 1 \leq i \leq k$$

where for any matrix $M$, $M'$ denotes $M$ with the first row deleted.

We claim that the collection of forms in $u$ comprising the entries of $F_u(x_i)$ and $JF_u(x_i)$ across all $i$, $1 \leq i \leq k$, is independent. Forms arising from different components of $F_u$ involve disjoint subsets of the coefficients in $u$, so it suffices to consider the case where $F_u$ is a single polynomial $f$ of degree $d > 2$. Let $\overline{f}$ denote the homogenization of $f$ and $\overline{x_i}$ denote the point in $\mathbb{P}^n$ with projective coordinates $[x_i; 1]$. Note that since the vectors $x_1, \ldots, x_k$ are affinely independent, the points $\overline{x_1}, \ldots, \overline{x_k}$ span a $(k-1)$-dimensional subspace of $\mathbb{P}^n$ as in the statement of Lemma 4.17. Suppose to the contrary that a relation of the form $\sum_{i=1}^k \alpha_i f(x_i) = \sum_{1 \leq i \leq k, 1 \leq j \leq n} \beta_{ij} \frac{\partial f}{\partial y_j}(x_i)$ holds. Then the same relation holds substituting $\overline{f}$ for $f$ and $\overline{x_i}$ for $x_i$. By Euler's formula, $d\overline{f}(\overline{x_i}) = \sum_{j=1}^{n+1} (\overline{x_i})_j \frac{\partial \overline{f}}{\partial y_j}(\overline{x_i})$. So we obtain a relation which contradicts Lemma 4.17 and Proposition 4.18.

We see that $\pi^{-1}(x_1, \ldots, x_k, t_1, \ldots, t_k)$ is a proper intersection of $k$ determinantal varieties which, by standard results, have codimension $n - c$ and a linear space defined by the linear forms $F_u(x_i)$ for $1 \leq i \leq k$. Altogether, the codimension of the fiber is $k(n - c + c) = kn$. $\square$

**Lemma 4.20.** Let $k \geq 2$ and $(d_1, \ldots, d_c) \in \mathbb{N}^c$ such that each $d_i > 2$ and let $S_k$ and $\Gamma_k$ be as in Definition 4.13. Then $\dim(S_k \setminus \pi^{-1}(\Gamma_k)) = \dim(U)$.

*Proof.* Consider the image of $\pi : (S_k \setminus \pi^{-1}(\Gamma_k)) \to (\prod_{i=1}^k \mathbb{C}^n) \times \mathbb{C}^k$, $V = \pi(S_k \setminus \pi^{-1}(\Gamma_k))$. One can easily see that $V$ is the open algebraic subset comprised of all $(x_1, \dots, x_k, t_1, \dots, t_k)$ where

$$\sum_{i=1}^k t_i = 1, \quad z = \sum_{i=1}^k t_i x_i, \quad d(x_1, z)^2 = d(x_j, z)^2, \quad 2 \le j \le k,$$

the $x_1, \dots, x_k$ are affinely independent, and none of the $t_i$ are 0. We claim that $V$ has codimension $k$, i.e., dimension $kn$. In fact, the $V$ is birationally equivalent to $\prod_{i=1}^k \mathbb{C}^n$. The forward morphism is given by the projection map $g : V \to \prod_{i=1}^k \mathbb{C}^n$ where $g(x_1, \dots, x_k, t_1, \dots, t_k) = (x_1, \dots, x_k)$. Setting $P$ to be the $n \times k$ matrix whose columns are the vectors with coordinates $x_1, \dots, x_k$, the inverse $h : \prod_{i=1}^k \mathbb{C}^n \to V$ is given by taking $h(x_1, \dots, x_k)$ to be $(x_1, \dots, x_k, t_1(P), t_2(P), \dots, t_k(P))$ where the functions $t_i(P)$ are rational functions yielding the barycentric coordinates of the circumcenter of the simplex whose vertices are the columns of $P$ (see, e.g., [32, Thm. 2.1.1] and [57, pp. 707–708]).

By Lemma 4.19, the fiber of $\pi^{-1}(z)$ has codimension $kn$ for any $z \in V$. It follows that $\dim(S_k \setminus \pi^{-1}(\Gamma_k)) = \dim(V) + \dim(\pi^{-1}(z)) = kn + (\dim(U) - kn) = \dim(U)$. □

Building on these results, we now present the proof of Theorem 4.14.

*Proof of Theorem 4.14.* If $c = n$, the complete intersection $X_u$ itself is finite and Theorem 4.14 is immediate, so assume that $c < n$. We may reduce to the case where none of the equations defining $X_u$ are linear. Indeed, for a generic hyperplane $H \subseteq \mathbb{C}^n$ there is a linear map which preserves algebraic $k$-bottlenecks of $X_u$ while eliminating a variable. After repeatedly removing linear equations we have by assumption that $d_i > 2$ for all $i$.

Let $S$ be an irreducible component of $S_k \setminus \pi^{-1}(\Gamma_k)$. By Lemma 4.20, $\dim S \le \dim U$. If $\eta_{|S}$ does not dominate $U$, then $S \cap \eta^{-1}(u)$ is empty for general $u \in U$. However, if $\eta_{|S}$ dominates $U$, then $\dim S = \dim U$ and $\eta^{-1}(u)$ is finite for general $u \in U$. □

# 5 Computational experiments for feature sizes

This Section contains results from computing the reach, bottlenecks, and weak feature size of examples of co-dimension 1 in $\mathbb{R}^2$ and co-dimensions 1 and 2 in $\mathbb{R}^3$. Data results and code for reproducing these computations are available at https://github.com/P-Edwards/wfs-and-reach-examples.

**Example 5.1.** Consider the "butterfly curve" in $\mathbb{R}^2$, which is the real part of the algebraic variety defined as $V(F) \cap \mathbb{R}^2$ where $F = x^4 - x^2y^2 + y^4 - 4x^2 - 2y^2 - x - 4y + 1$. This example has been considered before, e.g., by Brandt and Weinstein [13].

The algebraic medial axis for the butterfly curve was computed using numerical algebraic geometry and found to be irreducible of degree 120. The real part of this curve is shown in Figure 8(a) with the pieces in cyan forming the geometric medial axis. A lower bound of 0.103 on the reach was estimated with a homotopy continuation method based on Corollary 3.11 in agreement with [13, Ex. 6.1]. The points computed via Corollary 3.11 on the geometric medial axis are shown in red in Figure 8(b).

To compute the weak feature size of $V(F) \cap \mathbb{R}^2$, we used the numerical algebraic geometry method in Corollary 4.10. For both $k = 2$ and $k = 3$, the results indicate that the irreducible components of $B_k(F)$ not contained in $\Gamma_k$ are all isolated points, i.e., $V(F)$ has finitely many algebraic bottlenecks. The following table provides a summary of the outputs. Using a 24-CPU computer with just a standard 2-homogeneous homotopy, these computations took about 3 seconds for $k = 2$ and about 2.5 minutes for $k = 3$. In particular, the weak feature size of $V(F) \cap \mathbb{R}^2$ was determined to be approximately 0.251 and is attained by a geometric 2-bottleneck (cf., [13, Ex. 6.1]). Figures 9 and 10 show various types of bottlenecks for the butterfly curve.

| | $k = 2$ | $k = 3$ |
|---|---|---|
| Number of paths tracked using a 2-homogeneous homotopy | 1024 | 16384 |
| Number of points on $B_k(F)$ computed | 392 | 2817 |
| Number of computed points in $\Gamma_k$ | 200 | 1089 |
| Algebraic $k$-bottlenecks of $V(F)$ | 96 | 288 |
| Real algebraic $k$-bottlenecks of $V(F)$ | 26 | 28 |
| Real algebraic $k$-bottlenecks of $V(F) \cap \mathbb{R}^2$ | 22 | 17 |
| Geometric $k$-bottlenecks of $V(F) \cap \mathbb{R}^2$ | 3 | 2 |

**Example 5.2.** As an example of a non-quadratic complete intersection where Theorem 4.14 holds, consider the intersection of a torus and Clebsch surface in $\mathbb{R}^3$ defined by

$$F = \begin{bmatrix} (R^2 - r^2 + x^2 + y^2 + z^2)^2 - 4R^2(x^2 + y^2) \\ x^3 + y^3 + z^3 + 1 - (x + y + z + 1)^3 \end{bmatrix}$$

with $R = \frac{3}{2}$ and $r = 1$. In particular, the second equation is an algebraic surface with all 27 exceptional lines contained in $\mathbb{R}^3$ [24]. This curve is illustrated in Figure 11.

We computed the weak feature size for this curve by using homotopy continuation to compute $B_k(F)$ for $k = 2, 3, 4$. The computations indicated that the irreducible components of $B_k(G)$ not contained in $\Gamma_k$ are all isolated points. The weak feature size is approximately 0.405, which is attained at a geometric 2-bottleneck. In particular, this example of computing

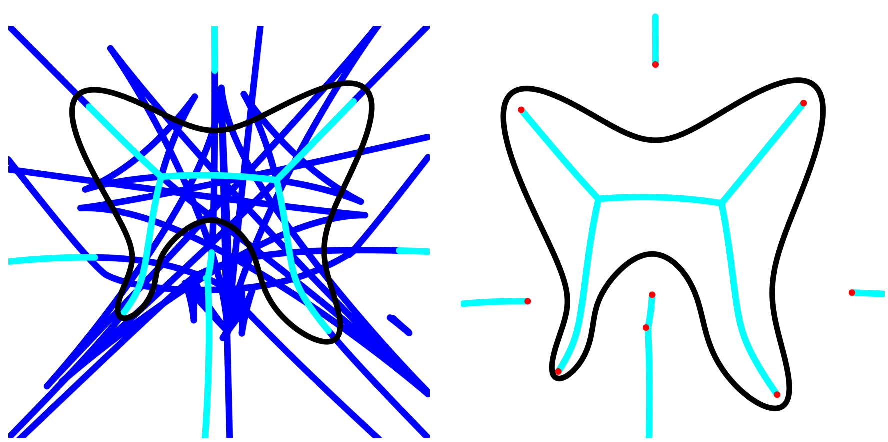

(a) (b)

Figure 8: For butterfly curve: (a) algebraic and geometric medial axis; (b) geometric medial axis with critical points.

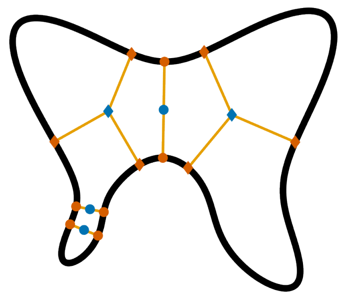

Figure 9: Geometric 2-bottlenecks (dark blue circles) and 3-bottlenecks (dark blue diamonds) of the butterfly curve. Orange dots are distance minimizers and connect to bottlenecks with light orange lines.

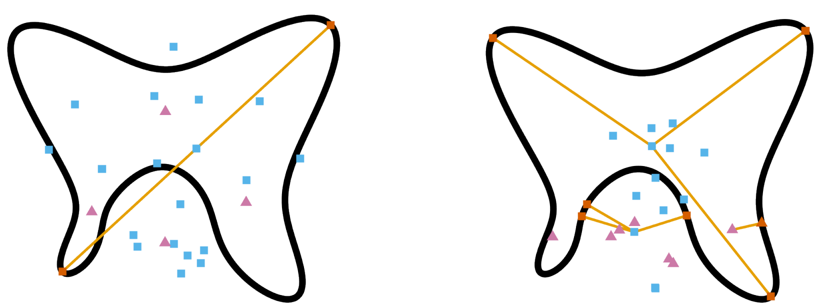

Figure 10: Algebraic 2-bottlenecks (left) and 3-bottlenecks (right) of the butterfly curve. Algebraic bottlenecks are blue and real algebraic bottlenecks of the butterfly curve are pink. For an illustrative subset, orange distance-critical points are connected to their corresponding bottleneck by orange lines.

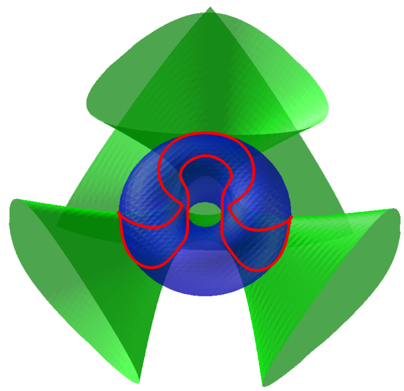

Figure 11: Curve (red) at the intersection of a torus (blue) and Clebsch surface (green).

the weak feature size is the most complicated we will consider in terms of computational cost. The cost of computing bottlenecks increases substantially with higher bottleneck order, both due to increasing the ambient dimension of $B_k(F)$ and because there are $k!$ solutions in $B_k(F)$ for each algebraic $k$-bottleneck. Regeneration methods [42] were used to make computations for this example more tractable. In particular, the 4-bottlenecks required approximately one week of computation on a 24-CPU computer. The table below summarizes the results.

| | $k=2$ | $k=3$ | $k=4$ |
|---|---|---|---|
| Number of points on $B_k(F)$ computed | 2736 | 94548 | 1431936 |
| Number of computed points in $\Gamma_k$ | 576 | 2424 | 0 |
| Algebraic $k$-bottlenecks of $V(F)$ | 1080 | 15354 | 59664 |
| Real algebraic $k$-bottlenecks of $V(F)$ | 68 | 324 | 586 |
| Real algebraic $k$-bottlenecks of $V(F) \cap \mathbb{R}^3$ | 50 | 134 | 86 |
| Geometric $k$-bottlenecks of $V(F) \cap \mathbb{R}^3$ | 22 | 6 | 0 |

**Example 5.3.** We conclude this collection of examples with the quartic surface in $\mathbb{R}^3$ from [29, §5.2] illustrated in Figure 12 and defined by

$$F = 4x^4 + 7y^4 + 3z^4 - 3 - 8x^3 + 2x^2y - 4x^2 - 8xy^2 - 5xy + 8x - 6y^3 + 8y^2 + 4y.$$

As in the previous examples, we computed that $V(F)$ has finitely many algebraic bottlenecks of orders 2 and 3. Since computing 4-bottlenecks proved similarly expensive to Example 5.2, they were not computed for this example.

This surface exhibits interesting behavior from an algebraic viewpoint. A point $p$ approximated by $(0.458, -0.97, 0)$ was computed to be the only geometric 2-bottleneck of $V(F) \cap \mathbb{R}^3$ as shown in Figure 12. The two corresponding points in $\rho_2^{-1}(p) \subseteq B_2(F)$ are isolated in the bottleneck correspondence but are singular, i.e., have multiplicity higher than 1. The weak feature size of approximately 0.354 is attained at $p$ with Figure 12 also showing the two geometric 3-bottlenecks. The following table summarizes this computation.

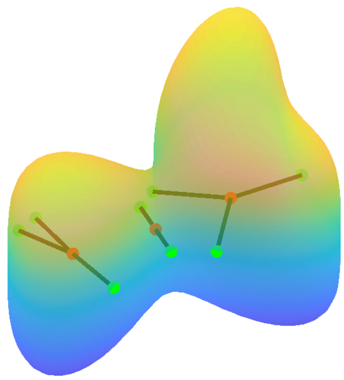

Figure 12: Quartic surface with geometric 2- and 3-bottlenecks

| | $k = 2$ | $k = 3$ |
|---|---|---|
| Number of points on $B_k(F)$ computed | 2220 | 40672 |
| Number of computed points in $\Gamma_k$ | 0 | 8191 |
| Geometric $k$-bottlenecks of $V(F) \cap \mathbb{R}^3$ | 1 | 2 |

# 6 Conclusion

In this paper, we developed theoretical foundations and numerical algebraic geometry methods for computing geometric feature sizes of algebraic manifolds. This study is not intended to be exhaustive, so some further questions both in terms of theory and applications follow.

**Real algebraic spaces with singularities.** It is natural to ask how the results presented here may generalize to singular spaces. Since isolated singularities can contribute additional irreducible components to $B_k(F)$, the impact of singularities must be analyzed.

**Counting algebraic bottlenecks.** A direct consequence of Theorem 4.14, which will be familiar to readers who have worked with parameter homotopies, is that, for a fixed degree pattern, there exist upper bounds on the number of algebraic (and so geometric) bottlenecks that apply for any generic algebraic manifold with that degree pattern. Computing sharp upper bounds, however, is an open problem of more than intrinsic interest. As an example of the geometric meaning of these bounds, consider a compact algebraic hypersurface $H \subseteq \mathbb{R}^n$, not necessarily smooth, e.g., the discriminant locus of a parameterized family. Thus, $\mathbb{R}^n \setminus H$ decomposes into a finite number of disconnected $n$-cells and the number of geometric bottlenecks of $H$ is an upper bound on the number of cells. Altogether, having good bounds on this number both for algebraic manifolds and for singular algebraic spaces could be useful for geometric algorithms which look to estimate the number and size of these cells.

**Reducing redundant computations.** For any polynomial system $F$, there is an action of the symmetric group on $k$ elements on the bottleneck correspondence $B_k(F)$. Namely, a permutation acts on an element $(x_1, \ldots, x_k, t_1, \ldots, t_k)$ by permuting both the $x_i$ and $t_i$. In the generic case when all non-degenerate solutions are isolated, standard homotopy continuation methods whose results we saw in this manuscript compute $k!$ solutions in $B_k(F)$ for each algebraic bottleneck. Is there a natural approach, e.g., building on methods utilized in [41, 58, 59], that takes advantage of the symmetry to reduce these redundancies?

# Acknowledgements

PBE thanks Antonio Lerario for interesting discussions, and both Parker Ladwig and Robert Goulding for help tracking down and verifying Cassini's study of his eponymous ovals. JDH was supported in part by NSF grant CCF-181274. OG was supported in part by EPSRC EP/R018472/1 and Bristol Myers Squibb. SDR was partially supported by the VR grant [NT:2018-03688]. 

# References

[1] E. Aamari, J. Kim, F. Chazal, B. Michel, A. Rinaldo, and L. Wasserman. Estimating the reach of a manifold. *Electron. J. Stat.*, 13(1):1359–1399, 2019.

[2] J. Alexander and A. Hirschowitz. Polynomial interpolation in several variables. *J. Algebraic Geom.*, 4(2):201–222, 1995.

[3] N. Amenta and M. Bern. Surface reconstruction by voronoi filtering. *Discrete & Computational Geometry*, 22(4):481–504, 1999.

[4] D. Attali, A. Lieutier, and D. Salinas. Vietoris-Rips complexes also provide topologically correct reconstructions of sampled shapes. *Comput. Geom.*, 46(4):448–465, 2013.

[5] S. Basu. Computing the first few Betti numbers of semi-algebraic sets in single exponential time. *Journal of Symbolic Computation*, 41(10):1125–1154, 2006.

[6] S. Basu and S. Percival. Efficient computation of a semi-algebraic basis of the first homology group of a semi-algebraic set. arXiv:2107.08947, 2021.

[7] D. J. Bates, D. Eklund, J. D. Hauenstein, and C. Peterson. Excess intersections and numerical irreducible decompositions. In *2021 23rd International Symposium on Symbolic and Numeric Algorithms for Scientific Computing (SYNASC)*, pages 52–60, 2021.

[8] D. J. Bates, J. D. Hauenstein, T. M. McCoy, C. Peterson, and A. J. Sommese. Recovering exact results from inexact numerical data in algebraic geometry. *Experimental Mathematics*, 22(1):38–50, 2013.

[9] D. J. Bates, J. D. Hauenstein, C. Peterson, and A. J. Sommese. Numerical decomposition of the rank-deficiency set of a matrix of multivariate polynomials. In *Approximate Commutative Algebra*, Texts Monogr. Symbol. Comput., pages 55–77. Springer, Vienna, 2009.

[10] D. J. Bates, J. D. Hauenstein, A. J. Sommese, and C. W. Wampler. *Numerically solving polynomial systems with Bertini*, volume 25. SIAM, 2013.

[11] D. J. Bates, J. D. Hauenstein, A. J. Sommese, and C. W. Wampler. Bertini: Software for numerical algebraic geometry. Available at bertini.nd.edu with permanent doi: dx.doi.org/10.7274/R0H41PB5, 2014.

[12] O. Bobrowski and R. J. Adler. Distance functions, critical points, and the topology of random Čech complexes. *Homology Homotopy Appl.*, 16(2):311–344, 2014.

[13] M. Brandt and M. Weinstein. Voronoi cells in metric algebraic geometry of plane curves. *arXiv preprint arXiv:1906.11337*, 2019.

[14] P. Breiding and S. Timme. The reach of a plane curve. https://www.JuliaHomotopyContinuation.org/examples/reach-curve/. Accessed: January 21, 2022.

[15] P. Breiding and S. Timme. Homotopycontinuation.jl: A package for homotopy continuation in julia. In J. H. Davenport, M. Kauers, G. Labahn, and J. Urban, editors, *Mathematical Software – ICMS 2018*, pages 458–465, Cham, 2018. Springer International Publishing.

[16] P. Bürgisser, F. Cucker, and P. Lairez. Computing the homology of basic semialgebraic sets in weak exponential time. *J. ACM*, 66(1):Art. 5, 30, 2019. [Publication date initially given as 2018].

[17] C. Carathéodory. Über den variabilitätsbereich der fourier'schen konstanten von positiven harmonischen funktionen. *Rendiconti Del Circolo Matematico di Palermo (1884-1940)*, 32(1):193–217, 1911.

[18] G. Carlsson. Topology and data. *Bulletin of the American Mathematical Society*, 46(2):255–308, 2009.

[19] J.-D. Cassini. *De l'Origine et du progrès de l'astronomie et de son usage dans la géographie et dans la navigation*. L'Imprimerie Royale, 1693. Accessed online 2021-05-27, https://gallica.bnf.fr/ark:/12148/bpt6k1510911j/f13.item, page 36.

[20] F. Chazal, D. Cohen-Steiner, and A. Lieutier. A sampling theory for compact sets in euclidean space. *Discrete & Computational Geometry*, 41(3):461–479, 2009.

[21] F. Chazal and A. Lieutier. Weak feature size and persistent homology: computing homology of solids in $\mathbb{R}^n$ from noisy data samples. In *Proceedings of the twenty-first annual symposium on Computational geometry*, pages 255–262. ACM, 2005.

[22] F. Chazal and A. Lieutier. Smooth manifold reconstruction from noisy and non-uniform approximation with guarantees. *Comput. Geom.*, 40(2):156–170, 2008.

[23] F. Chazal and B. Michel. An introduction to topological data analysis: Fundamental and practical aspects for data scientists. *Frontiers in Artificial Intelligence*, page 108, 2021.

[24] A. Clebsch. Ueber die Anwendung der quadratischen Substitution auf die Gleichungen 5 $^{ten}$ Grades und die geometrische Theorie des ebenen Fünfseits. *Math. Ann.*, 4(2):284–345, 1871.

[25] D. Cohen-Steiner, H. Edelsbrunner, and J. Harer. Stability of persistence diagrams. *Discrete Comput. Geom.*, 37(1):103–120, 2007.

[26] T. K. Dey, X. Ge, Q. Que, I. Safa, L. Wang, and Y. Wang. Feature-preserving reconstruction of singular surfaces. In *Computer Graphics Forum*, volume 31, pages 1787–1796. Wiley Online Library, 2012.

[27] S. Di Rocco, D. Eklund, and O. Gäfvert. Sampling and homology via bottlenecks. *Mathematics of Computations, to appear*, 2022.

[28] S. Di Rocco, D. Eklund, and M. Weinstein. The bottleneck degree of algebraic varieties. *SIAM J. Appl. Algebra Geom.*, 4(1):227–253, 2020.

[29] E. Dufresne, P. Edwards, H. Harrington, and J. Hauenstein. Sampling real algebraic varieties for topological data analysis. In *2019 18th IEEE International Conference On Machine Learning And Applications (ICMLA)*, pages 1531–1536. IEEE, 2019.

[30] D. Eklund. The numerical algebraic geometry of bottlenecks. *Advances in Applied Mathematics*, 142:102416, 2023.

[31] H. Federer. Curvature measures. *Trans. Amer. Math. Soc.*, 93:418–491, 1959.

[32] M. Fiedler. *Matrices and graphs in geometry*, volume 139 of *Encyclopedia of Mathematics and its Applications*. Cambridge University Press, Cambridge, 2011.

[33] J. H. G. Fu. Tubular neighborhoods in Euclidean spaces. *Duke Math. J.*, 52(4):1025–1046, 1985.

[34] V. Gershkovich and H. Rubinstein. Morse theory for Min-type functions. *Asian J. Math.*, 1(4):696–715, 1997.

[35] R. Ghrist. Barcodes: the persistent topology of data. *Bulletin of the American Mathematical Society*, 45(1):61–75, 2008.

[36] B. Giunti. Tda-applications: A database for application of tda outside of maths. `https://www.zotero.org/groups/2425412/tda-applications`. Accessed: August 2022.

[37] K. Grove. Critical point theory for distance functions. In *Differential geometry: Riemannian geometry (Los Angeles, CA, 1990)*, volume 54 of *Proc. Sympos. Pure Math.*, pages 357–385. Amer. Math. Soc., Providence, RI, 1993.

[38] K. Grove and K. Shiohama. A generalized sphere theorem. *Ann. of Math. (2)*, 106(2):201–211, 1977.

[39] O. Hanner. Some theorems on absolute neighborhood retracts. *Ark. Mat.*, 1:389–408, 1951.

[40] J. D. Hauenstein. Numerically computing real points on algebraic sets. *Acta Applicandae Mathematicae*, 125:105–119, 2013.

[41] J. D. Hauenstein, L. Oeding, G. Ottaviani, and A. J. Sommese. Homotopy techniques for tensor decomposition and perfect identifiability. *Journal für die reine und angewandte Mathematik (Crelles Journal)*, 2019(753):1–22, 2019.

[42] J. D. Hauenstein, A. J. Sommese, and C. W. Wampler. Regeneration homotopies for solving systems of polynomials. *Math. Comp.*, 80(273):345–377, 2011.

[43] J. D. Hauenstein, A. J. Sommese, and C. W. Wampler. Regenerative cascade homotopies for solving polynomial systems. *Applied Mathematics and Computation*, 218(4):1240–1246, 2011.

[44] F. Hensel, M. Moor, and B. Rieck. A survey of topological machine learning methods. *Frontiers in Artificial Intelligence*, 4:681108, 2021.

[45] E. Horobeţ. The critical curvature degree of an algebraic variety. *arXiv preprint arXiv:2104.01124*, 2021.

[46] E. Horobeţ and M. Weinstein. Offset hypersurfaces and persistent homology of algebraic varieties. *Computer Aided Geometric Design*, 74:101767, 2019.

[47] J. Kim, J. Shin, F. Chazal, A. Rinaldo, and L. Wasserman. Homotopy reconstruction via the Cech complex and the Vietoris-Rips complex. In *36th International Symposium on Computational Geometry*, volume 164 of *LIPIcs. Leibniz Int. Proc. Inform.*, pages Art. No. 54, 19. Schloss Dagstuhl. Leibniz-Zent. Inform., Wadern, 2020.

[48] S. Lojasiewicz. Triangulation of semi-analytic sets. *Ann. Scuola Norm. Sup. Pisa Cl. Sci. (3)*, 18:449–474, 1964.

[49] J. Milnor. *Morse theory.* Annals of Mathematics Studies, No. 51. Princeton University Press, Princeton, N.J., 1963. Based on lecture notes by M. Spivak and R. Wells.

[50] A. P. Morgan and A. J. Sommese. Coefficient-parameter polynomial continuation. *Appl. Math. Comput.*, 29(2, part II):123–160, 1989.

[51] A. P. Morse. The behavior of a function on its critical set. *Ann. of Math. (2)*, 40(1):62–70, 1939.

[52] M. Morse. *The calculus of variations in the large*, volume 18. American Mathematical Soc., 1934.

[53] P. Niyogi, S. Smale, and S. Weinberger. Finding the Homology of Submanifolds with High Confidence from Random Samples. *Discrete & Computational Geometry*, 39(1-3):419–441, 2008.

[54] A. Sard. The measure of the critical values of differentiable maps. *Bull. Amer. Math. Soc.*, 48:883–890, 1942.

[55] A. J. Sommese and J. Verschelde. Numerical homotopies to compute generic points on positive dimensional algebraic sets. *Journal of Complexity*, 16(3):572–602, 2000.

[56] A. J. Sommese and C. W. Wampler, II. *The Numerical Solution of Systems of Polynomials Arising in Engineering and Science*. World Scientific Publishing Co. Pte. Ltd., Hackensack, NJ, 2005.

[57] E. VanderZee, A. N. Hirani, D. Guoy, V. Zharnitsky, and E. A. Ramos. Geometric and combinatorial properties of well-centered triangulations in three and higher dimensions. *Comput. Geom.*, 46(6):700–724, 2013.

[58] J. Verschelde and R. Cools. Symmetric homotopy construction. *Journal of Computational and Applied Mathematics*, 50(1):575–592, 1994.

[59] C. W. Wampler, A. P. Morgan, and A. J. Sommese. Complete Solution of the Nine-Point Path Synthesis Problem for Four-Bar Linkages. *Journal of Mechanical Design*, 114(1):153–159, 1992.

[60] L. Wasserman. Topological data analysis. *Annual Review of Statistics and Its Application*, 5(1):501–532, 2018.

[61] R. C. Yates. *A Handbook on Curves and Their Properties*. J. W. Edwards, Ann Arbor, Michigan, 1947.